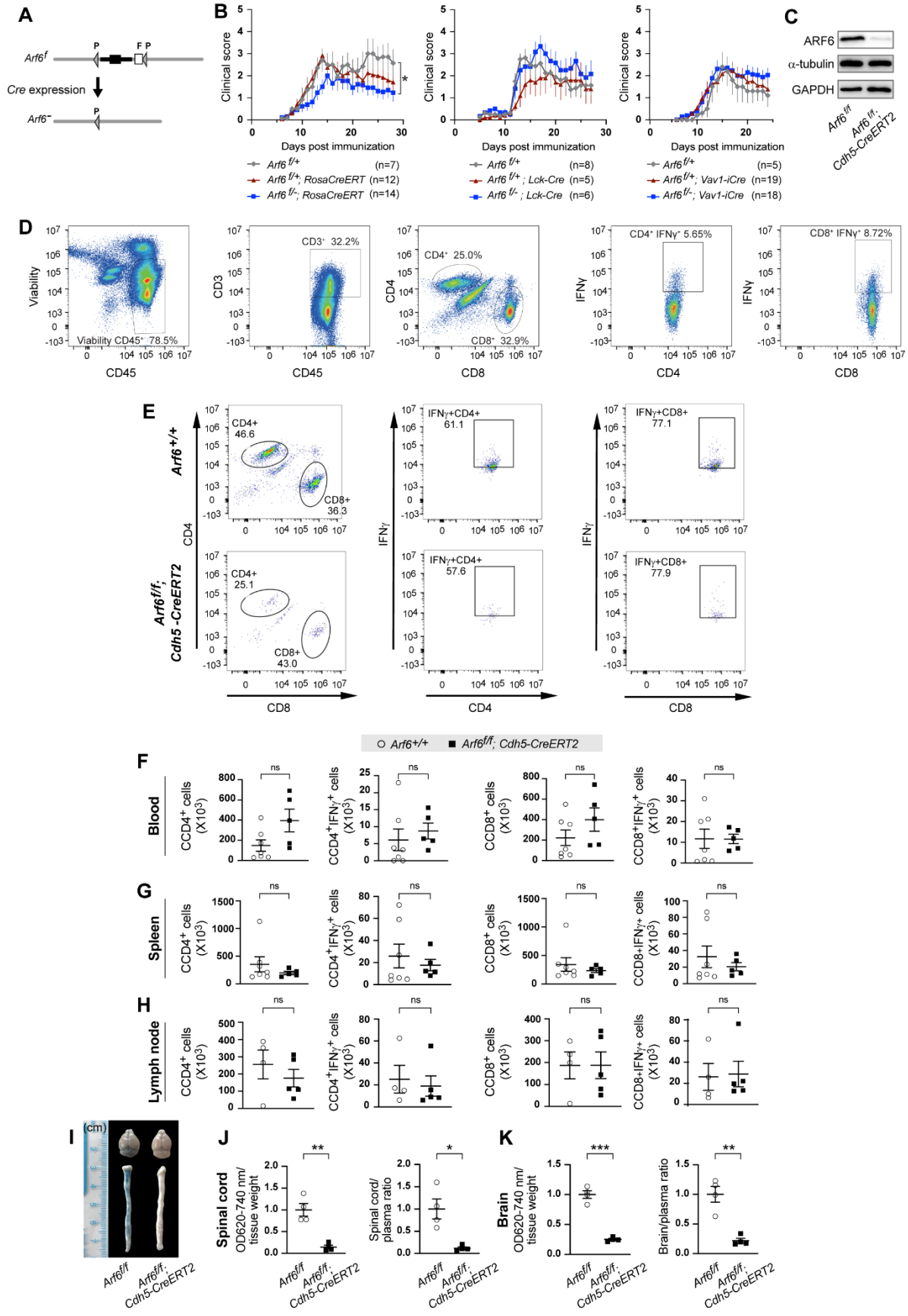
A
Arf6f
P
F P
Cre expression
Arf6−
P
B
Clinical score
Days post immunization
Arf6 f/+ (n=7)
Arf6 f/+; RosaCreERT (n=12)
Arf6 f/-; RosaCreERT (n=14)
Arf6 f/+ (n=8)
Arf6 f/+ ; Lck-Cre (n=5)
Arf6 f/- ; Lck-Cre (n=6)
Arf6 f/+ (n=5)
Arf6 f/+; Vav1-iCre (n=19)
Arf6 f/-; Vav1-iCre (n=18)
C
ARF6
α-tubulin
GAPDH
Arf6f/f
Arf6f/f; Cdh5-CreERT2
D
Viability
Viability CD45+ 78.5%
CD45
CD3+ 32.2%
CD3
CD4+ 25.0%
CD8+ 32.9%
CD4
CD4+ IFNγ+ 5.65%
IFNγ
CD8+ IFNγ+ 8.72%
CD8
E
Arf6+/+
Arf6f/f; Cdh5 -CreERT2
CD4+ 46.6
CD8+ 36.3
CD4+ 25.1
CD8+ 43.0
CD8
IFNγ+CD4+ 61.1
IFNγ+CD4+ 57.6
CD4
IFNγ+CD8+ 77.1
IFNγ+CD8+ 77.9
IFNγ
Arf6+/+
Arf6f/f; Cdh5-CreERT2
F
Blood
CCD4+ cells (X10³)
CCD4+IFNγ+ cells (X10³)
CCD8+ cells (X10³)
CCD8+IFNγ+ cells (X10³)
ns
G
Spleen
CCD4+ cells (X10³)
CCD4+IFNγ+ cells (X10³)
CCD8+ cells (X10³)
CCD8+IFNγ+ cells (X10³)
ns
H
Lymph node
CCD4+ cells (X10³)
CCD4+IFNγ+ cells (X10³)
CCD8+ cells (X10³)
CCD8+IFNγ+ cells (X10³)
ns
I
(cm)
Arf6f/f
Arf6f/f; Cdh5-CreERT2
J
Spinal cord
OD620-740 nm/ tissue weight
Spinal cord/ plasma ratio
**
*
Arf6f/f
Arf6f/f; Cdh5-CreERT2
K
Brain
OD620-740 nm/ tissue weight
Brain/plasma ratio
***
**
Arf6f/f
Arf6f/f; Cdh5-CreERT2

Figure S1 (Related to Figure 1). Further characterization of EAE mice with *Arf6* loss produced by various Cre-recombinase drivers. (A) Schematic of modified *Arf6* alleles. (B) EAE clinical scores in whole-body *Arf6* knockout mice (*Arf6*$^{fl/-}$; *Rosa-CreERT*), T cell-specific *Arf6* knockout mice (*Arf6*$^{f/-}$*; LckCre*), and hematopoietic cell-specific *Arf6* knockout mice (*Arf6*$^{f/-}$*; Vav-iCre*). Two-way ANOVA with Šidák's correction for multiple comparisons. *$p<0.05$ (corrected for multiple comparisons using Holm-Šidák's method). (C) Validation of endothelial-specific *Arf6* knockout from lysates of lung endothelial cells. (D) Representative flow plots from spleen showing gating strategy used for data shown in Figure 1D. (E) Example of flow cytometry used to measure the number of spinal cord $CD4^+$, $CD4^+IFN\gamma^+$, $CD8^+$, $CD8^+IFN\gamma^+$ T-cells in endothelial-specific *Arf6* knockout EAE mice and their littermates at day 28 post-MOG immunization. (F-H) The total number of $CD4^+$, $CD4^+IFN\gamma^+$, $CD8^+$, $CD8^+IFN\gamma^+$ T-cells in the blood, spleen, and lymph nodes of endothelial-specific *Arf6* knockout EAE mice and their littermates were measured by flow cytometry on day 28 post-MOG immunization. Two-tailed Student's *t* test or Mann-Whitney test depending on whether data appear to be normally distributed. ns: not significant. All error bars represent the SEM. (I-K) Vascular leak in the brain and spinal cord of *Arf6*$^{f/f}$ and *Arf6*$^{f/f}$; *Chd5-CreERT2* mice at 21 days post-immunization. (I) Brain and spinal cord images illustrating amount of vascular leak for each genotype. (J and K) Vascular leak analyzed using both a common method (left panel) and an approach in which the spinal cord:plasma and brain:plasma ratios of Evans blue are determined (right panel). Two-tailed Welch's t test. Both methods produce similar results, indicating that endothelial loss of *Arf6* significantly reduces vascular leak.

Figure S2
Sun, Z. et al.

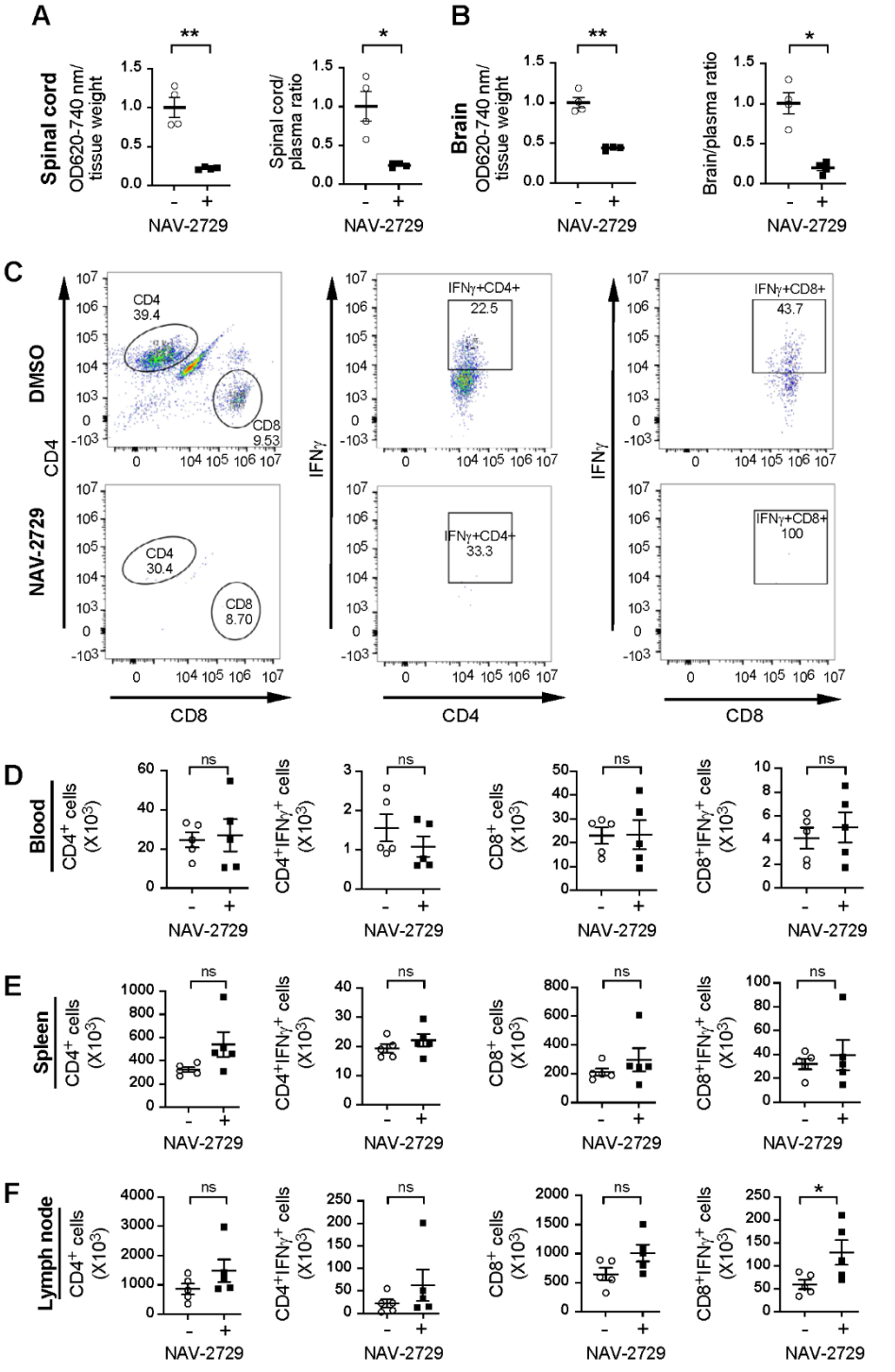

Figure S2 (Related to Figure 2). Characterization of EAE mice treated with an ARF6 inhibitor. Spinal cord (A) and brain (B) vascular leak studies using both a common method (left panel) and an approach in which the spinal cord:plasma and brain:plasma ratios of Evans blue are determined (right panel). Two-tailed Welch's t test. Both methods produce similar results indicating that ARF6 inhibition by NAV-2729 significantly reduces vascular leak. (C) Representative flow plots from spinal cords showing gating strategy used for data shown in Figure 2G. (D-F) Mice were treated with NAV-2729 starting at 13 days post-immunization. The total number of $CD4^+$, $CD4^+IFN\gamma^+$, $CD8^+$, $CD8^+IFN\gamma^+$ T-cells within the blood, spleen, and lymph nodes of EAE mice were measured by flow cytometry on day 28 post-MOG immunization. n=5 mice per group. Two-tailed Student's *t* test, Welch's t test, or Mann-Whitney test depending on whether variances are approximately equal and data appear to be normally distributed. ns: not significant.

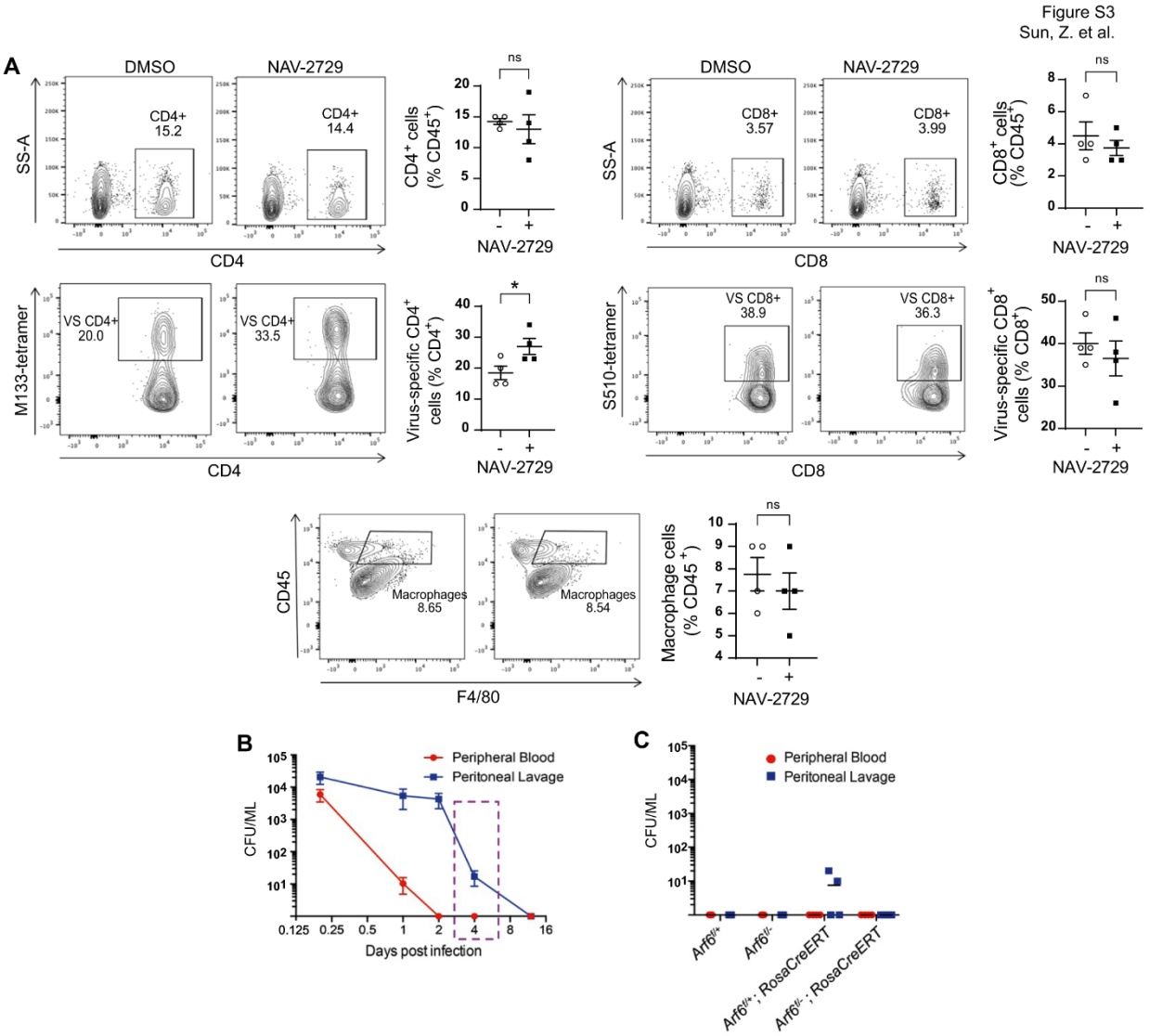

Figure S3 (Related to Figure 2). Further characterization of EAE mice treated with an ARF6 inhibitor and viable immune responses in mice with loss of *Arf6*. (A) ARF6 inhibitor NAV-2729 was IP injected every other day for 10 days beginning 24 hours after JHMV infection. Total $CD4^+$ and $CD8^+$ T-cells, virus-specific $CD4^+$ and $CD8^+$ T-cells, and macrophages were measured on day 14 post infection. n=4 mice per group. (B) C57BL/6 mice were injected intraperitoneally with a fecal bacteria slurry to determine the correct time point (dotted box) for experiment shown in panel G. Bacteria in peripheral blood and peritoneal lavage were measured over time. (C) Whole-body *Arf6* knockout mice were injected intraperitoneally with a fecal bacteria slurry. Peripheral blood and peritoneal lavage bacteria were measured 4-days post infection. n=3-4 per group. Two-tailed Student's *t* test (panels B-E). *p<0.05, ns: not significant. All error bars represent the SEM.

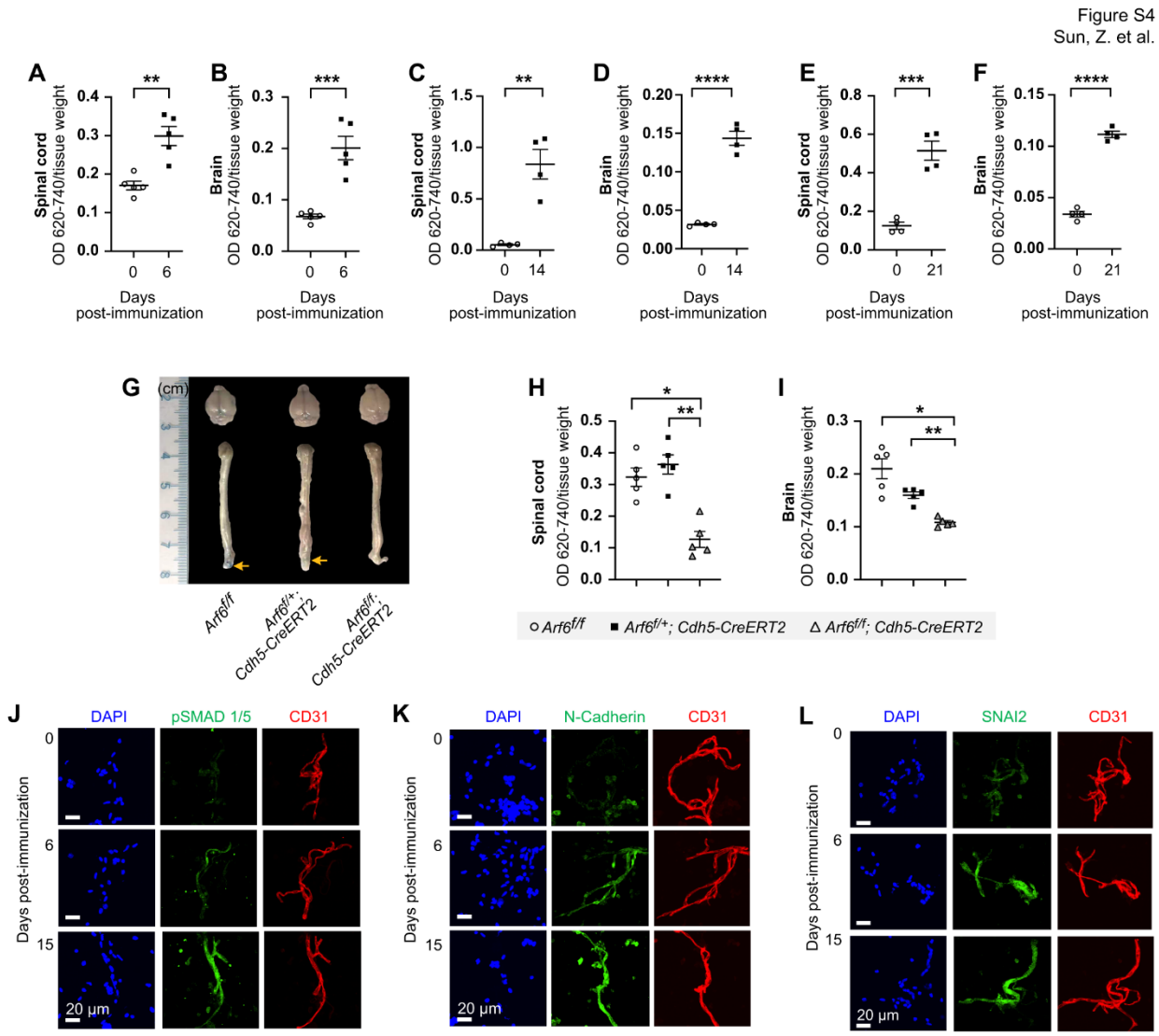

Figure S4 (Related to Figure 3). EAE-induced vascular leakage in the CNS and EndoMT. (A-F) Amount of Evans blue dye found in spinal cord and brain parenchymal tissues at 0 and 6 days (A and B), 0 and 14 days (C and D), and 0 and 21 days (E and F) post-EAE induction in wild-type mice as measured by absorbance at OD 620 and 740 (n=4 or 5 mice per group).(G) Evans blue dye present in the brain and caudal region of the spinal cord (arrows) in *Arf6*$^{f/f}$ and *Arf6*$^{f/+}$*; Cdh5-CreERT2* mice but absent in *Arf6*$^{f/f}$*; Cdh5-CreERT2* at 6 days post-immunization. (H and I) Quantification of results shown in panel G (n=5 mice per group). (J-L) Supporting data for Figure 3D showing unmerged individual images for each marker.

Figure S5
Sun, Z. et al.

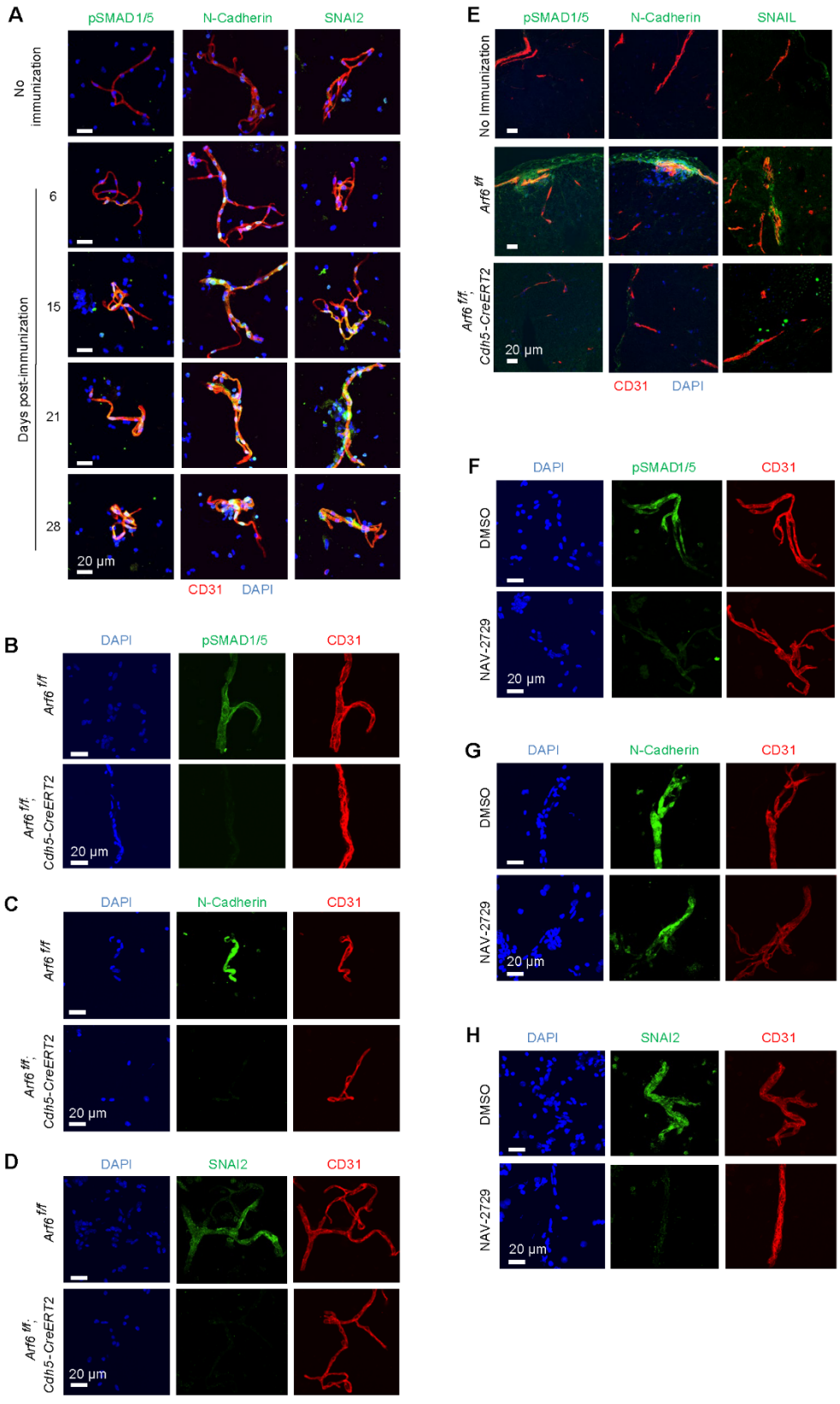

Figure S5 (Related to Figure 3). Time course of EAE-induced EndoMT and effects of ARF6 loss or inhibition on EndoMT in EAE mice. (A) EndoMT in isolated spinal cord microvessels at 6, 15, 21, and 28 days post-EAE induction was assessed by examining pSMAD1/5, N-Cadherin, and SNAI2 expression using immunofluorescence. (B-D) Supporting data for Figure 3F showing unmerged individual images for each marker. (E) EndoMT in spinal cord tissue sections at 28 days post-EAE induction was assessed by examining pSMAD1/5, N-Cadherin, and SNAIL expression using immunofluorescence. (F-H) Supporting data for Figure 3H showing unmerged individual images for each marker.

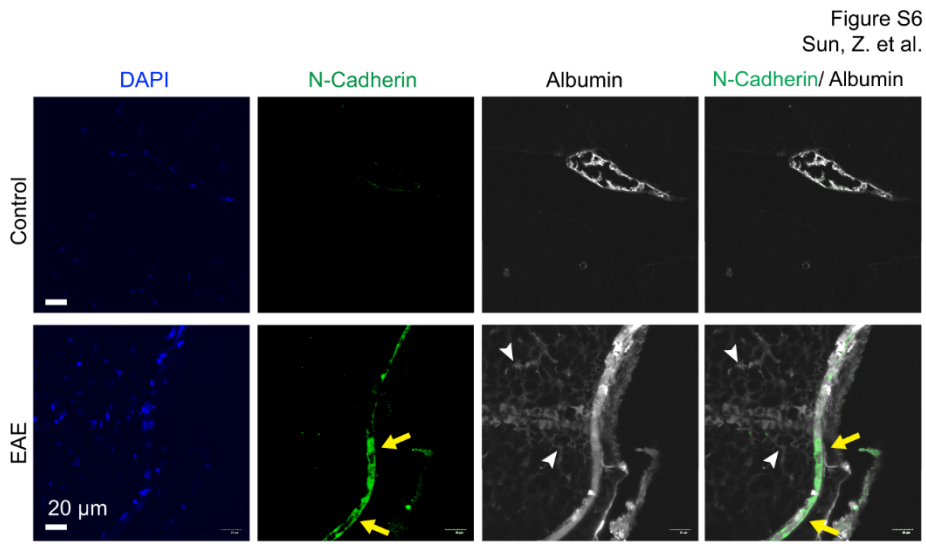

Figure S6 (Related to Figure 3). Association of vascular leakage with EndoMT. Vascular leak is associated with EndoMT in EAE-induced mice. In the lower row of images, yellow arrows point to blood vessels that show evidence of EndoMT (N-cadherin expression, green fluorescence). White arrowheads point to Alexa fluor™ 647-labeled albumin (white fluorescence) that has leaked from the blood vessels into the spinal cord parenchyma. Upper row shows an albumin-containing blood vessel with no evidence of EndoMT or vascular leak.

Figure S7
Sun, Z. et al.

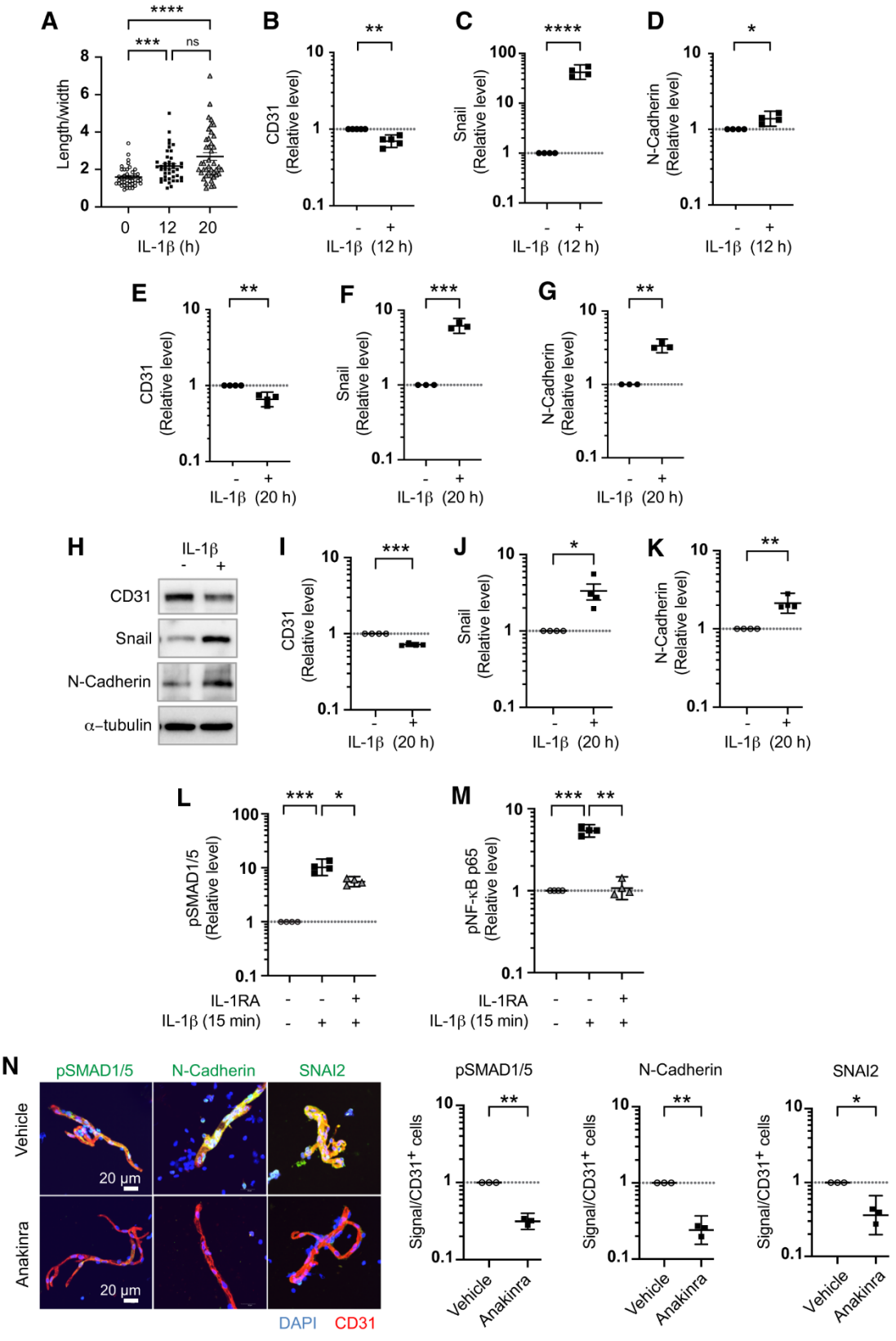

Figure S7 (Related to Figure 4). The role of IL-1β in EndoMT in human and mouse brain microvascular endothelial cells and EAE-induced EndoMT in mice. (A) Morphological changes in HBMECs treated with IL-1β as measured by changes in the length to width ratio. Each data point represents a different cell (n=42 cells per group). Welch's one-way ANOVA with Dunnett's T3 multiple comparisons test. (B-G) Quantification of western blots from IL-1β-induced (12 h or 20 h) EndoMT in HBMECs that are represented in Figure 4B (n=3-5). (H-K) IL-1β treatment (150 ng/mL for 20 h) induces EndoMT in MBMECs as evidenced by downregulation of CD31 and upregulation of Snail and N-cadherin (n=4). (L, M) IL-1β induces activation of SMAD1/5 (pSMAD1/5) in human brain endothelial cells, which can be partially blocked with IL-1RA. pNF-κB acts as a positive control for IL-1β signaling. Quantification of representative western blot shown in Figure 4D (n=4). (N) Blocking IL-1β signaling *in vivo* using anakinra (pharmaceutical grade IL-1RA) inhibits EndoMT in EAE mice as evidenced by downregulation of EndoMT markers pSMAD1/5, N-cadherin, and SNAI2 in isolated spinal cord blood vessels using immunofluorescent labeling (n=3). Ratio paired t tests were used for panels B-G, I-K, and N. One-way randomized block ANOVA with Tukey's multiple comparisons test following $\log_{10}$ transformation of the data for panels L and M. Geometric means and 95% confidence intervals are shown.

Figure S8
Sun, Z. et al.

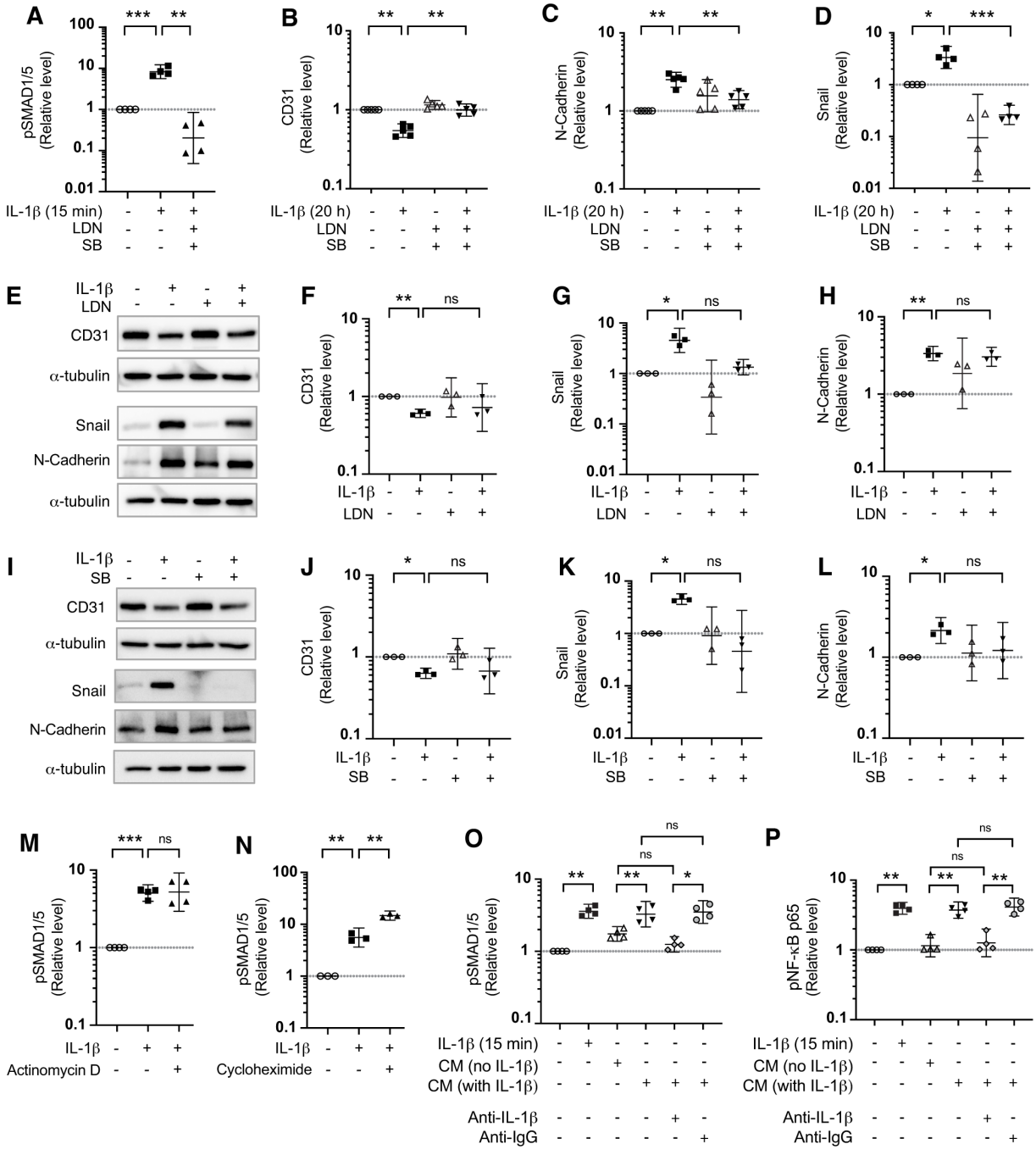

Figure S8 (Related to Figure 4). Efficient blocking of EndoMT requires pan-ALK inhibtion; RNA and protein synthesis as well as secretion of ALK ligands are not required for IL-1β-induced activation of SMAD1/5. (A-D) Quantification of western blots represented in Figure 4E and 4F showing that pan-ALK inhibition using a combination of LDN and SB efficiently inhibits EndoMT in HBMECs. (E-H) Western blot and quantification showing that the ALK inhibitor LDN does not efficiently inhibit IL-1β-induced EndoMT in HBMECs. (I-L) Western blot and quantification showing that the ALK inhibitor SB does not efficiently inhibit IL-1β-induced EndoMT in HBMECs. (M, N) Quantification of western blots represented in Figure 4G showing that inhibition of RNA transcription with actinomycin-D and protein synthesis with cycloheximide does not block IL-1β-induced activation of SMAD1/5 (n=3 or 4). (O, P) Quantification of western blots represented in Figure 4H showing that IL-1β-induced SMAD1/5 in human brain endothelial cells does not require the secretion of ALK ligands and extracellular activation of ALKs (n=4). NF-κB acts as a positive control for IL-1β signaling and anti-IgG acts as a negative control for anti-IL-1β. CM=conditioned medium. One-way randomized block ANOVA with Tukey's multiple comparisons test following $\log_{10}$ transformation (panels B-D, F-H, and J-P). Geometric means and 95% confidence intervals are shown.

Figure S9
Sun, Z. et al.

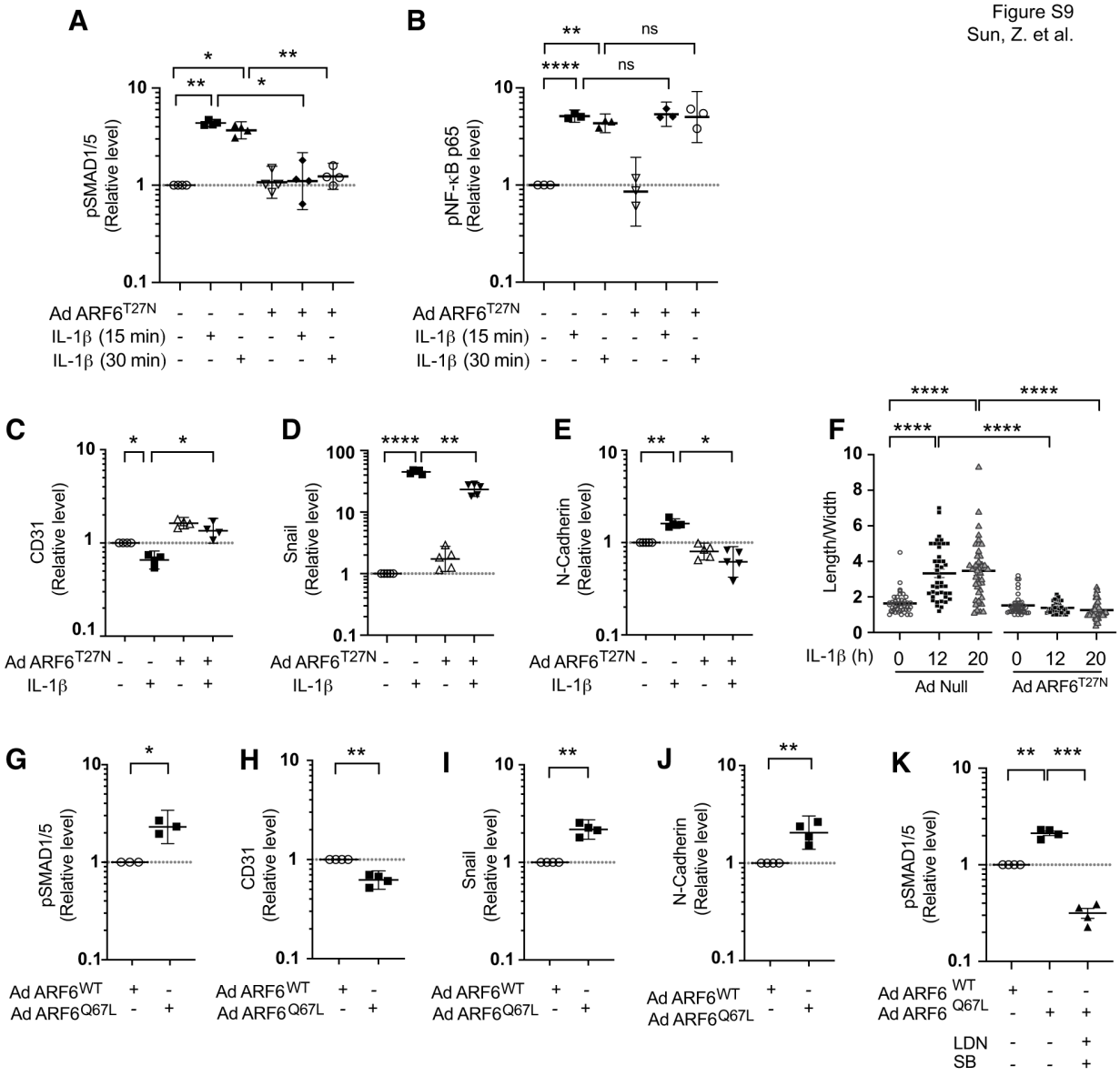

Figure S9 (Related to Figure 5). Dominant-negative ARF6 inhibits both IL-1β-induced EndoMT and morphological changes in human brain microvascular endothelial cells, while EndoMT that is induced by constitutively active ARF6 is blocked pan-ALK inhibition. (A-E) Quantification of western blots represented in Figure 5C and 5D showing that dominant-negative ARF6 ($ARF6^{T27N}$) inhibits IL-1β-induced EndoMT but not NF-κB activation (n=3-5). (F) Dominant-negative ARF6 ($ARF6^{T27N}$) blocks IL-1β-induced morphological changes (i.e., cellular elongation) in HBMECs. Each data point represents a different cell (n=42 cells per group). Welch's one-way ANOVA with Dunnett's T3 multiple comparisons test. (G-J) Quantification of western blots represented in Figure 5F showing that constitutively active ARF6 ($ARF6^{Q67L}$) induces EndoMT in HBMECs as evidenced by a decrease in CD31 expression with a concomitant increase in SMAD1/5 activation and Snail and N-cadherin expression (n=3 or 4). (K) Quantification of western blots represented in Figure 5G showing that pan-ALK inhibition with LDN and SB blocks constitutively active ARF6 ($ARF6^{Q67L}$)-induced SMAD1/5 activation (n=4). One-way randomized block ANOVA with Tukey's multiple comparisons test following $\log_{10}$ transformation (panels A-E and K) and ratio paired t test (panels G-J). Geometric means and 95% confidence intervals are shown.

Figure S10
Sun, Z. et al.

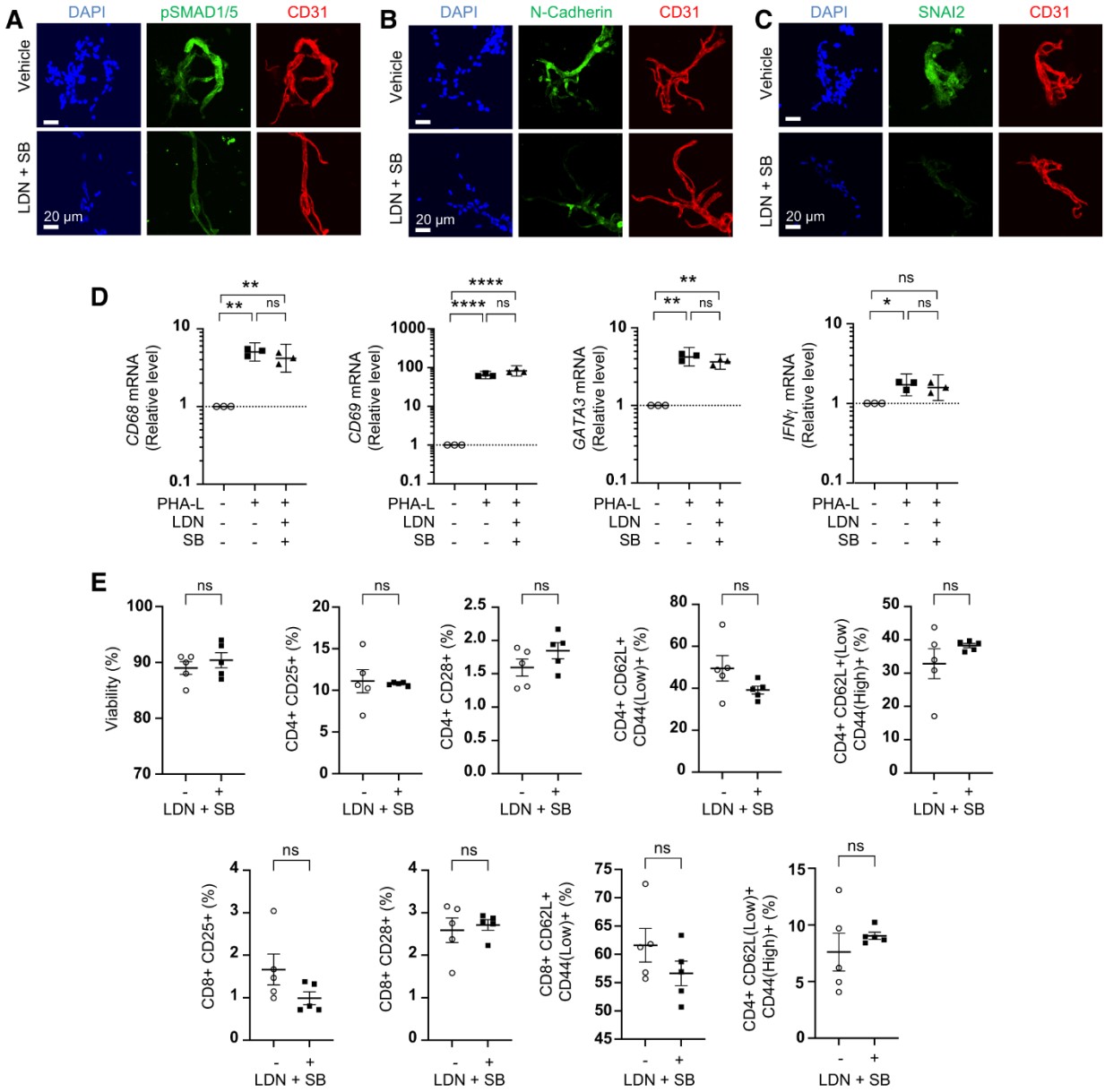

Figure S10 (Related to Figure 6). Pan-ALK inhibition has little effect on the immune response yet can inhibit EAE-induced EndoMT in mice. (A-C) Supporting data for Figure 6D and 6E showing unmerged individual images for each EndoMT marker in EAE mice treated with the ALK inhibitors LDN and SB. (D) Quantitative RT-PCR of markers indicative of T cell activation (*CD68*, *CD69*, *GATA3*, and *IFNγ*) in phytohemagglutinin (PHA-L)-activated T cells treated with or without ALK inhibitors LDN and SB (n=3). (E) *In vivo* assessment of the effect of pan-ALK inhibition (LDN + SB) in EAE mice on T cell viability and percentages of specific T cell types that are associated with EAE showing that there are no statistically significant changes in mice treated with the ALK inhibitors (n=5).